Journal of Materials Chemistry A

Molecular simulation study on the flexibility in the interpenetrated metal–organic framework LMOF-201 using reactive force field

Journal:	*Journal of Materials Chemistry A*
Manuscript ID	TA-ART-11-2019-012065.R3
Article Type:	Paper
Date Submitted by the Author:	13-Jul-2020
Complete List of Authors:	Agrawal, Ankit; Tokyo Daigaku, Department of Mechanical Engineering Agrawal, Mayank; Brown University, School of Engineering Suh, Donguk; Tokyo Daigaku, Department of Mechanical Engineering Ma, Yunsheng; Nagoya University, of Chemistry and Biotechnology, School of EngineeringDepartment Matsuda, Ryotaro; Nagoya University Endo, Akira; National Institute of Advanced Industrial Science and Technology (AIST), Hsu, Wei-Lun; Tokyo Daigaku, Department of Mechanical Engineering Daiguji, Hirofumi; Tokyo Daigaku, Department of Mechanical Engineering

Molecular simulation study on the flexibility in the interpenetrated metal–organic framework LMOF-201 using reactive force field

Received 00th January 20xx,
Accepted 00th January 20xx

DOI: 10.1039/x0xx00000x

Ankit Agrawal, [a] Mayank Agrawal, [b] Donguk Suh [a], Yunsheng Ma, [c,d] Ryotaro Matsuda, [c] Akira Endo, [e] Wei-Lun Hsu, [a] and Hirofumi Daiguji*[a]

Framework flexibility is one of the most important characteristics of metal–organic frameworks (MOFs), making them highly suitable for adsorption applications. There have been a limited number of computational efforts to study flexible MOFs in the literature, and they are mostly focused on MIL-53. We studied a flexible MOF known as LMOF-201, which was found to exhibit guest-induced flexible properties; however, the mechanism of the appearance of flexibility is still unclear. First, we validated our simulation results by reproducing the experimental isotherm and powder X-ray diffraction measurements of experimental structures using grand canonical Monte Carlo (GCMC) and reactive force field (ReaxFF) molecular dynamics (MD) simulations. Then, we demonstrated the importance of the presence of a carbonyl oxygen atom in LMOF-201 to induce flexibility. The mechanism determined in this study will enable LMOF-201 to be considered for adsorption applications in the future.

Introduction

Metal–organic frameworks (MOFs) have been considered to be one of the most promising porous materials for gas adsorption. They have been attracting widespread interest owing to their good stability, high porosity, and the convenient customizability of their pore diameter, pore volume, and surface area.[1,2] In addition to these fundamental characteristics of MOFs, “flexibility” is a further special feature considered to be advantageous for adsorption applications.[3,4] Flexibility is defined as the change in the structure of the MOFs due to a stimulus. These stimuli include the adsorption of guest molecules and the change in temperature or pressure. In a recent literature review on this topic by Alijammal et al.[5] several aspects of flexibility concerning MOFs are presented in detail. Several types of flexibility behaviour have been reported in MOFs:[6] 1) negative thermal expansion, 2) breathing, 3) gate-opening, and 4) swelling. There are several experimental techniques to detect the structural transformations in flexible MOFs. However, the main experimental problem is that the analysis of structure transitions occurring at the microscopic level is complicated. Thus, molecular simulations become necessary to comprehend these changes at the molecular level.

Several studies have been conducted to identify the types of structural changes and the factors these originate from. The series of MIL-53 frameworks are the most commonly computationally studied and well documented flexible MOFs for a variety of adsorbates.[7–15] The MIL-53 series (=Al and Cr) have been found to exhibit a breathing behaviour and a reversible structural change between the narrow (NP) and large (LP) pore forms, when exposed to guest molecules. Salles et al.[10] performed a systematic study on MIL-53 (Cr) and developed a robust flexible force field to efficiently obtain the structural response of MIL-53(Cr) under CO_2 adsorption. They used consistent valence force field (CVFF) parameters for organic moiety, and the missing parameters were obtained by an empirical fitting approach based on energy minimization. They captured the dynamics of MIL-53 under the effect of CO_2 adsorption and obtained the NP, transient and LP structures from molecular dynamics (MD) simulations. Their results were in excellent agreement with those of the experiments and demonstrated that the change in the dihedral angle was the predominant reason of the structural switching. The flexible force field parameters for this approach are generally obtained from generic force fields, such as CVFF, universal force field (UFF), or Dreiding force field, while the unavailable parameters are derived or tuned using an empirical fitting approach or quantum mechanical (QM) calculations.[8] However, the limitation of this approach is that tuning or deriving the force field parameters to describe the flexibility of the MOF is time consuming and computationally demanding. Furthermore, flexible force fields, also known as bonded force fields, previously developed in the literature are applicable only for special materials that have an identical atomistic structure as the material the parameters are derived for. The bonded force field parameters are essential to run MD simulations which provide the information about the different structures for a

[a] Department of Mechanical Engineering, The University of Tokyo, 7-3-1 Hongo, Bunkyo-ku, Tokyo 113-8656, Japan. Email: daiguji@thml.t.u-tokyo.ac.jp
[b] School of Engineering, Brown University, Providence, Rhode Island 02912, United States
[c] Department of Applied Chemistry, Nagoya University, Furo-cho, Chikusa-ku, Nagoya, Aichi 464-8603, Japan
[d] School of Chemistry and Materials Engineering, Jiangsu Key Laboratory of Advanced Functional Materials, Changshu Institute of Technology, Changshu, Jiangsu 215500, PR China
[e] National Institute of Advanced Industrial Science and Technology (AIST), AIST Tsukuba Central 5-2, 1-1-1 Higashi, Tsukuba, Ibaraki 305-8565, Japan
†Electronic Supplementary Information (ESI) available. See DOI: 10.1039/x0xx00000x

given flexible MOF. These structures are used to further carry out GCMC simulations to obtain the adsorption isotherms. Bonded force field parameters for a given MOF cannot be easily transferred to other MOFs unlike non-bonded force field parameters, which limits the computational analysis of a greater variety of flexible MOFs.[16]

To tackle the problem with bonded force field transferability, researchers have suggested further techniques in which grand canonical Monte Carlo (GCMC) simulations are performed on different structures directly obtained from experiments, using a rigid framework approximation. As GCMC calculations only requires non-bonded force field parameters, the standard non-bonded force field parameters from UFF and Dreiding can be used which are valid for all types of MOFs irrespective of the material, it is being used for. There is no need of bonded force field to perform MD simulations as the distinct structures are already available from the experiments. Ramsahye et al.[7] and Perez et al.[11] conducted GCMC simulations on the experimentally obtained structures to model the adsorption in a flexible MIL-53(Al) and found the reason behind the flexibility. Another type of MOF, known as elastic layered structured framework-11 (ELM-11) was studied by Hiraide et al. for CO_2 separation, using the same technique.[17,18] They demonstrated that the gate opening behaviour of ELM-11 was due to the CO_2 adsorption and proposed the suitability of ELM-11 for practical applications owing to its high CO_2/N_2 selectivity. Although this approach is interesting, the main problem with this method is that extracting the crystal structure data of MOFs experimentally is not always feasible all the time. Therefore, there have been only a limited number of studies that computationally examined flexible MOFs despite the large number of actually synthesized MOFs.[19] Thus, the current research needs to be aimed on the better understanding of the physics and chemistry of adsorption in flexible MOFs.

In this study, we investigate the flexibility of LMOF-201, an interpenetrated luminescent MOF (LMOF), due to CO_2 adsorption. LMOFs are potential materials for chemical sensing and explosive detection.[20] They are particularly effective for luminescence applications owing to their permanent porosity, thermal stability, and guest-induced structural tuning.[21,22] Although all these properties are equally desirable for gas adsorption applications as well, LMOFs have not been widely adopted in this field. LMOF-201 was first reported by Hu et al., who applied it for the sensing of explosive RDX.[23] Ma et al.[24] studied both LMOF-201 and LMOF-202, which are both isostructural, but while LMOF-202 is rigid, LMOF-201 is flexible. They discovered that the flexibility of LMOF-201 was due to the addition of one carbonyl oxygen atom into the structure. Fig. 1 shows the crystal structures of LMOF-201 and LMOF-202 and their unit elements, 4,4'-bipyridine (bpy), 9-fluorenone-2,7-dicarboxylate (OFDC) and fluorene-2,7-dicarboxylate (FDC).

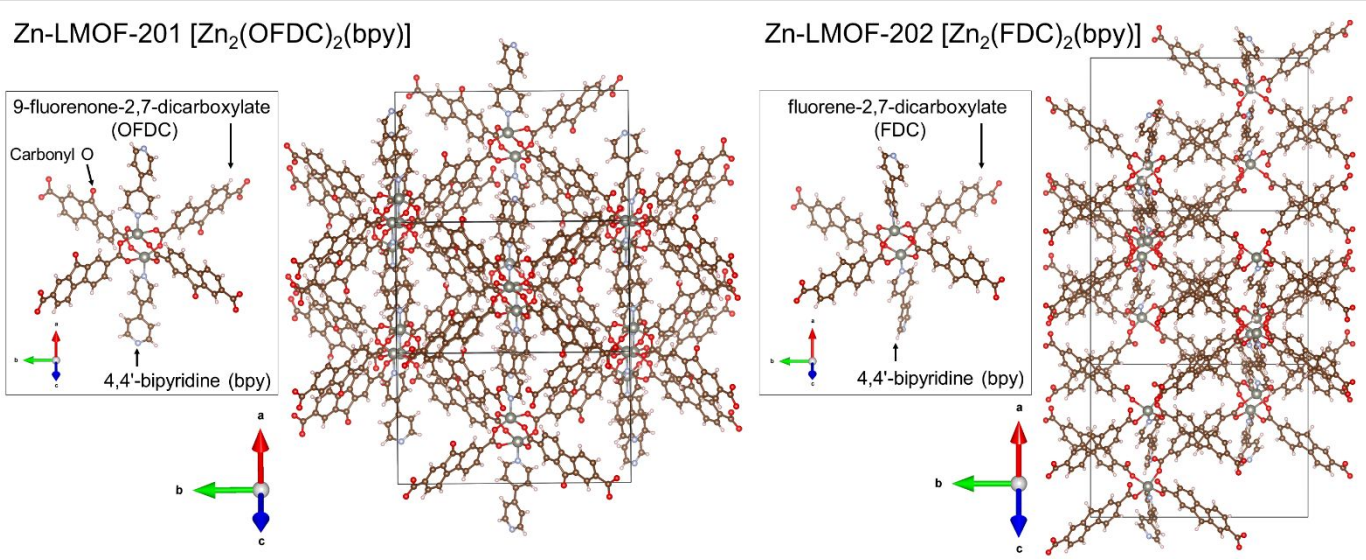

Fig. 1 Crystal structures of LMOF-201 and LMOF-202 and their unit elements, 4,4'-bipyridine (bpy), 9-fluorenone-2,7-dicarboxylate (OFDC) and fluorene-2,7-dicarboxylate (FDC)[24]

Powder X-ray diffraction (PXRD) measurements of LMOF-201 in adsorption measurements indicated the existence of two reversible structural changes similar to those of MIL-53. This flexibility doubled the amount of adsorbed CO_2 at saturation compared to that of LMOF-202 at 195 K. In spite of the fact that LMOF-201 can be a potential material for CO_2 adsorption and separation owing to its flexible characteristics, no efforts have been made so far to study the flexibility of LMOF-201. There is no information available on the two previously discovered distinct structures, and the microscopic mechanism responsible for flexibility is still not fully understood. Therefore, our aim is to investigate the flexibility inside LMOF-201 by using reactive force field (ReaxFF) combined with GCMC and MD simulations. Although, ReaxFF is mainly developed to model systems in which chemical reactions occur, it has also been applied to study the thermal stability of various MOFs with non-identical atomic arrangements and volume evolution of guest-induced MOF structures.[25–28] Considering its previous successful application, we employed ReaxFF to examine the guest-induced structural changes in LMOF-201. The objectives of the current work are as follows: (1) to reproduce previous experimental findings using simulations and (2) to identify the phenomena

occurring at the molecular level, resulting in the flexibility of LMOF-201.

Computational methods

GCMC simulations were carried out to obtain the adsorption isotherms for LMOF-201 using the RASPA simulation software.[29] Non-bonded interactions between the adsorbates and the framework atoms were calculated by employing the Lennard-Jones (L-J) potential with a cut-off distance of 12 Å. The Lorentz−Berthelot mixing rules were employed to determine the cross L-J parameters. The Dreiding force field parameters (UFF for metal atoms) were used for the framework atoms.[30,31] The TraPPE force field was used to model CO_2.[32] All parameters are listed in Tables S1 and S2 of the ESI.† To calculate the Coulombic forces, the electrostatic charges on atoms in the MOF were assigned on the entire periodic framework using the charge equilibration (Qeq) method as implemented in RASPA. We used equilibration and production periods of 5×10^4 and 1×10^5 Monte Carlo (MC) cycles, respectively. In each MC cycle, adsorbate insertion, deletion, rotation, and translation moves were implemented with equal probabilities of 0.25. The Coulombic interactions were calculated using the Ewald method with an Ewald precision of 10^{-6} and a cut-off of 12 Å.

The LMOF-201 single-crystal structure by Ma et al.[24] was used as the starting structure filled with the CO_2 molecules for the MD calculations. We considered the number of CO_2 molecules (N) based on the adsorption isotherm of LMOF-201 (0, 0.5, 0.875, 1, 4.75, and 5 CO_2/Zn). The adsorbate-loaded frameworks were prepared from GCMC simulations. The periodic cubic simulation box was a 1 × 1 × 1 unit cell of the LMOF-201 framework. The ReaxFF force fields provided by Professor Adri C.T. van Duin for C, H, O, N, and Zn atoms were employed for the MD simulations on LMOF-201 using LAMMPS molecular dynamics program.[33] For each CO_2 concentration, energy minimization was performed on the initial LMOF-201 configuration with the corresponding number of CO_2 molecules, and then the NPT-ensemble MD simulation was carried out at 195 K within 1.25 ns, followed by the production run for 0.25 ns. The system pressure was maintained at 1 atm. The time step was 0.25 fs and the temperature and pressure were controlled using a Nosé−Hoover thermostat/barostat with pressure and temperature damping constants of 25000 fs and 25 fs, respectively.

Results and discussion

Framework flexibility

Fig. 2 shows the experimental sorption LMOF-201 profiles at 195 K and the PXRD measurements of LMOF-201 measured under CO_2 sorption. Structure A represents the single-crystal structure, B is the as-synthesized LMOF-201 structure, and C is the guest-free structure obtained after drying the solvent molecules from the as-synthesized LMOF-201. It was found experimentally, that PXRD measurements of C and A were different, which suggested structural changes inside the LMOF-201. From points C to F, the consistent PXRD measurements suggest the existence of one structure. Furthermore, the additional peaks from points F to G in the PXRD measurements, indicate that a structural change occurred in this region. The identical PXRD measurements at points G and H confirm that a different structure exists in this region. A further result is that the initial structure of LMOF-201 was retained after desorption (point J).

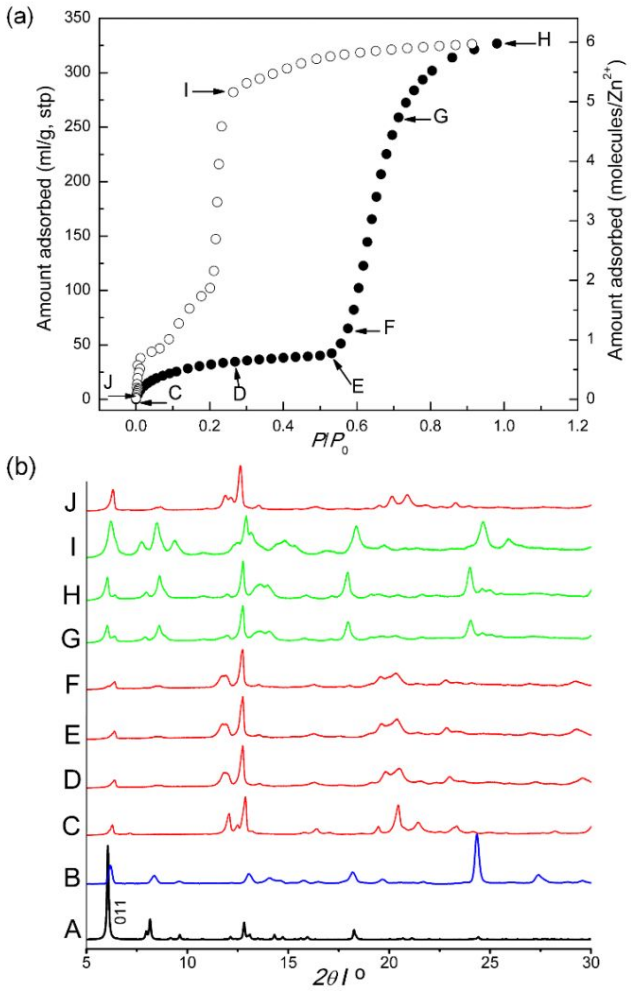

Fig. 2 (a) CO_2 adsorption (●) and desorption (○) profiles of LMOF-201 at 195 K. (b) A: simulated pattern of the single-crystal structure of LMOF-201, B: pattern of the as-synthesized LMOF-201 measured at ambient temperature, and C–J: PXRD patterns of LMOF-201 measured under CO_2 sorption. Each pattern corresponds to the points labeled in the isotherms. Cu-Kα radiation was used for all of the measurements. (Reproduced from Ref. 24 with permission from The Royal Society of Chemistry)

To computationally assess this occurrence, we first reproduced the experimental CO_2 adsorption isotherm of LMOF-201 by assuming a rigid structure. The isotherm resulting from applying the GCMC calculations on the rigid structure A is shown in Fig. S1 of the ESI.† As expected, the isotherm from the simulation does not match with the experimental one. The difference in the isotherms results from the structural change of the LMOF-201, which was not considered during the simulation, as the structure was considered to be rigid throughout the simulation.

Volume change with CO_2 loading

To consider the flexibility in the simulations, first we conducted NPT-MD simulations on LMOF-201 with different CO_2 amounts and measured the volume change of the structure at the corresponding concentration of CO_2 in a quasi-static process at 195 K and 1 atm. The change in the volume of the unit cell as a function of time at different CO_2 concentrations is shown in Fig. S2 of the ESI,† while Fig. 3 shows the unit cell volume with CO_2 loading. Structure P (3.418 nm^3) is a guest-free structure with a different unit cell volume than that of structure A (5.932 nm^3). This observation verifies the experimental prediction of the structural change after drying the sample (Fig. 2, structures A and C). Moving toward point R, it can be seen that the volume is constant up to a critical CO_2 concentration (point R). At point S (1 CO_2/Zn), there is a sharp increase in the volume, which indicates a change in the structure morphology. This critical CO_2 concentration value is in good agreement with the experimental values. Experimentally, it was revealed that the structural change started after 1.1 CO_2/Zn (Fig. 2, point F). From S to U (5 CO_2/Zn), the volume becomes nearly twice of that of structure P. This result from MD simulations complements the experimental discovery of the existence of different structures. We also performed NPT-MD simulations on LMOF-202, which was modelled by removing one carbonyl oxygen atom from LMOF-201, surprisingly the volume of LMOF-202 also changes with different CO_2 amounts. The progression of the LMOF-202 unit cell volume with CO_2 loading at 195 K is shown in Fig. S3 of the ESI.† However, the volume of LMOF-201 increases stepwise around n_{CO_2}/n_{Zn} = 1, while the volume of LMOF-202 increases smoothly with respect to n_{CO_2}/n_{Zn} in the entire range. This result suggests that ReaxFF cannot express the stiffness of LMOF-202 accurately but ReaxFF can capture the sudden expansion of the frame of LMOF-201 due to the presence of the carbonyl oxygen.

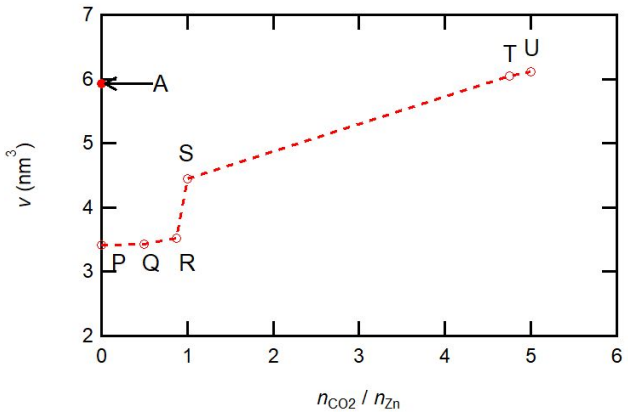

Fig. 3 Progression of the LMOF-201 unit cell volume with CO_2 loading at 195 K.

Adsorption isotherm of CO_2

The structural information from MD simulations enables the GCMC calculations on the structures obtained to determine the adsorption isotherm. We examined structures P and U for further GCMC calculations, which were analogous to the two distinct structures at low and high CO_2 loading respectively. We will refer to structure P as empty and U as full for simplicity. First, we determined the isotherm for individual structures and then combined them to obtain the complete isotherm. Fig. 4 shows the merged isotherm of the two structures. The complete isotherm is given by the structure P curve up to p/p_0 = 0.6 and then through a sharp jump, by the structure U curve. The isotherm obtained this way is in very good agreement with the experimental adsorption isotherm. However, the combined isotherm does not agree with the experimental results in the pressure region of 0.5–0.8, even though the structure P curve is in agreement with that of the experiments at $p/p_0 < 0.5$ and the structure U curve can accurately describe the experimental loading at $p/p_0 > 0.8$. The pressure region of 0.5–0.8 is the transition region. However, it is still unclear whether the experimental adsorption isotherm in this region can be attributed to the structure that constitutes the characteristics of two different structures or to the structure in a transition state that is evolving from one state to the other.

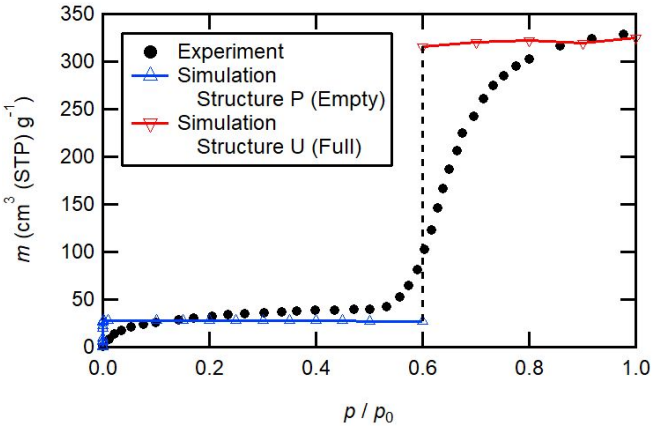

Fig. 4 Adsorption isotherm of CO_2 in LMOF-201 at 195 K (Experiments and simulations).

Guest induced flexibility mechanism

As our main aim was to demonstrate the guest induced flexibility mechanism inside LMOF-201, we studied the structures in more detail. Fig. 5(a) shows the three structures: A, P, and U (filled with CO_2). There is no H-bonding in structure A. While, in the structure P, hydrogen bonding exists only between the carbonyl oxygen and the surrounding hydrogen. The characteristic distances between this hydrogen and the carbonyl oxygen are 1.86 and 1.9 Å. As we move towards structure U, we observe that these carbonyl oxygen hydrogen bonds are being replaced by the hydrogen bonds to the oxygen of CO_2 molecules. While some carbonyl oxygen bonds are present, but the characteristic distance is increasing resulting in the opening up of the structure. In case of structure S, the oxygen of CO_2 molecules has superseded some of the carbonyl oxygen atoms to form hydrogen bonds and the characteristic distance is 1.93 Å for the remaining carbonyl oxygen hydrogen bonds. In structure U, the bond with carbonyl oxygen does not completely vanish but the characteristic distance between the hydrogen and the carbonyl oxygen has increased to 2.0 Å and, almost all the carbonyl oxygen atoms in the hydrogen bonds previously formed in P have been replaced by the hydrogen

bonds to the oxygen of CO_2 molecules. The whole mechanism can be interpreted as follows. Structure A contracts due to the H-bonding by the carbonyl oxygen and structure P is obtained. The strong interaction between the carbonyl oxygen and the framework keeps the structure shrunken, which results in lower porosity and CO_2 adsorption.

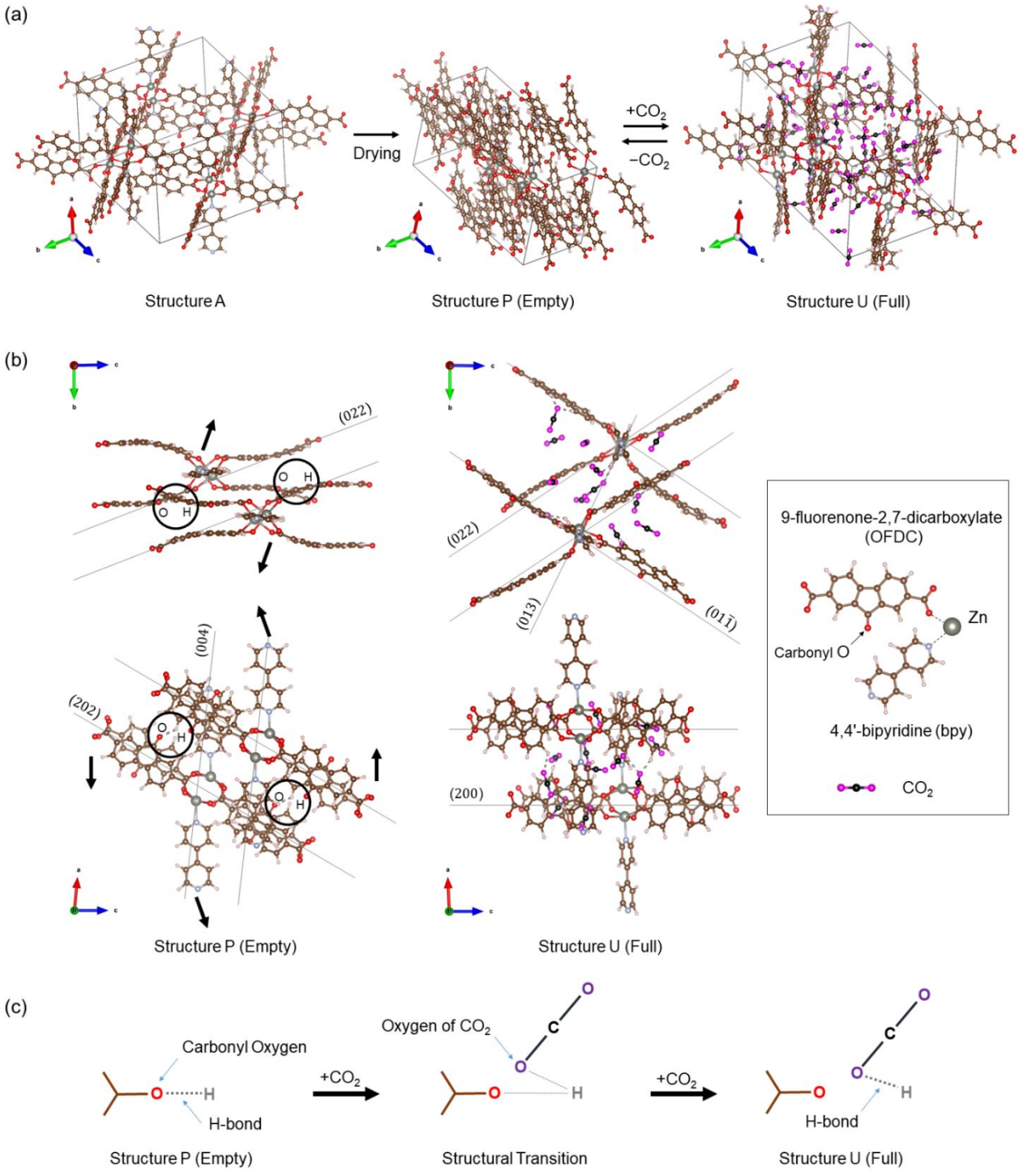

Fig. 5 (a) Structures A, P (Empty), and U (Full), (b) details of structures P (Empty) and U (Full), and (c) mechanism of the flexibility in LMOF-201.

Fig. 5(b) shows the detailed structure of structures P and U. Structure P exhibits a layered structure. The unit elements of LMOF-201, 4,4'-bipyridine (bpy), and 9-fluorenone-2,7-dicarboxylate (OFDC), are stacked in layers in the *b* direction and also well aligned along the [101] axis. The distances between the (202), (004), and (022) crystal planes are 6.28 Å, 6.23 Å, and 4.40 Å, respectively (equivalent to $2\vartheta = 14.1°$, 14.2°, and 20.2°, respectively, at $\lambda = 1.54$ Å). There are several other periodic structures on this length scale for structure P. As the CO_2 adsorption continues, more CO_2 molecules are filling the

system. These CO_2 molecules are interacting with the framework through the H-bonding and weakening the interaction between the carbonyl oxygen and the framework. Due to this H-bonding shift effect, the framework begins to expand, resulting in a larger adsorption capacity. Finally, structure U is obtained with a volume twice of that of structure P. As shown in Fig. 5(a), structure U is similar to structure A. The distance between the (011) crystal planes is 13.8 Å (equivalent to $2\vartheta = 6.4°$ at $\lambda = 1.54$ Å). This is the distance between bpy and OFDC and the space is created with the same size with or without CO_2 loading. Furthermore, by comparing structures P and U, we found that the unit cell did not expand homogeneously. The bpy and OFDC rotate around the axes *a*, *b*, and *c*, and at the same time, expand in all three directions, as shown in Fig. 5(b). As a result, the layered framework structure (structure P) changes to a three-dimensional jungle-gym-like framework structure (structure U). The H-bonding shift effect, that is, the mechanism begins at the framework expansion, is also in agreement with the previously mentioned experimental findings about the transformation from structure A to C as drying is performed. This is because when the solvent molecules are removed during the drying process, the carbonyl oxygen comes closer to the hydrogen atoms and forms H-bonds, resulting in structural contraction. The recovery of the structure to its original from after complete desorption is due to the same effect (Fig. 2, point J). The complete mechanism is shown in Fig. 5(c). The carbonyl oxygen is playing an important role in the flexibility as explained above, LMOF-202 doesn't have this carbonyl oxygen so there is no possibility of structure opening up or contracting due to hydrogen bonding, hence LMOF-202 is rigid.

The similarities between the PXRD measurement results of structures P and U and those of structures C and H substantiate our simulation results further. Fig. 6 shows the PXRD measurement results for structures obtained from the simulations (P and U) and those experimentally observed (C and H). Without CO_2 loading (Fig. 6(a)), several peaks appear around $2\vartheta \simeq 10°–15°$ in structure P. This result is due to the several fine periodic structures in the simulated framework, as mentioned before. Whereas in structure C, corresponding empty structure obtained from experiment, fewer peaks appear in this range. This might be partially because the periodicity was emphasized due to the limitation of the simulation cell and partially because the periodicity was underestimated due to the imperfection of the synthesized sample and the measurement. At low angle 2ϑ ($2\vartheta \simeq 6°–7°$), the molecular simulation results show that the peak without CO_2 loading can be attributed to the (101) crystal plane, the double of the distance between the (202) crystal planes, which is the distance between the stacked OFDCs. At high CO_2 loading (Fig. 6(b)), the peak at low angle 2ϑ can be attributed to the (011) crystal plane, which is the characteristic length scale of the porous structure of LMOF-201. The bpy and OFDC face each other with maintaining this distance. The 2ϑ peak intensity of the (101) crystal plane without CO_2 loading is slightly higher than that of the (011) crystal plane at high CO_2 loading, which is consistent with the experimental result. Although our results cannot be matched perfectly with the measurements, a number of the peaks can be distinguished that are in agreement with the experimental results. The experimental isotherm and PXRD measurements qualitatively agree with our simulation results.

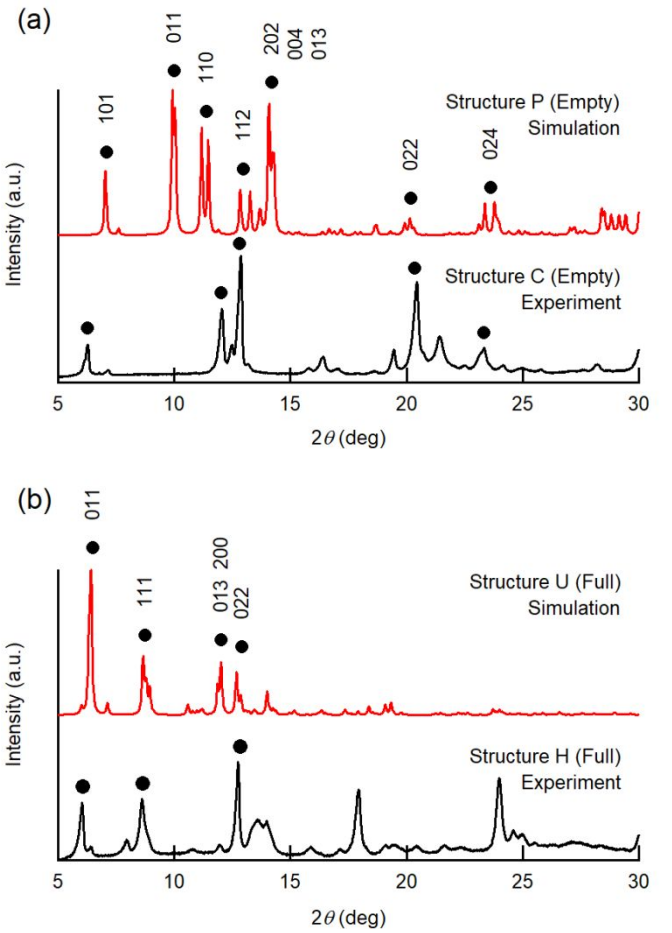

Fig. 6 Calculated and measured PXRD results (a) without CO_2 loading and (b) at high CO_2 loading.

Conclusions

This paper presents a study on the flexibility in LMOF-201. The GCMC calculations performed on LMOF-201 by assuming a rigid framework provided inconsistent results with the experimental values. By incorporating flexibility in LMOF-201 using ReaxFF, we provided comprehensive results, demonstrating the appearance of distinct structures. We successfully determined the CO_2 loading at which the variation in the structure initiates (simulation: 1 CO_2/Zn, experiment: 1.1 CO_2/Zn). The sudden breathing and experimental isotherm were reproduced appropriately in our simulations. The isotherm includes contribution of two forms in the relevant region. The similarities between the PXRD measurement results obtained from simulations and those obtained from experiments further support the findings of our simulations. Importantly, we found that the strong H-bonding due to the presence of the carbonyl oxygen in the LMOF-201 reproduces the stepwise volume change of the framework with CO_2 adsorption. However, there

are certain limitations associated with our force field as we are not able to capture the rigid nature of LMOF-202. Also, we have very limited information to cross validate our simulation results and force field unlike MIL-53. On the experimental side, the paper on which our computational study is based, to the best of our knowledge is the only paper in which the flexibility of LMOF-201 is studied. On the computational side, for the first time we are trying to realize the molecular level phenomena responsible for the flexibility of LMOF-201. MIL-53 has been studied for wide variety of adsorbates such as water, CO_2 etc. But in case of LMOF-201, it has been only been studied for CO_2 adsorption that too in only our experimental reference paper. All these factors point out that, in future there should be more research focused on LMOF-201.

This study is a first step towards our enhanced understanding of LMOF-201 and will stimulate the research to explore this material for adsorption applications. It should be noted that the inclusion of only one oxygen atom in LMOF-201 dramatically affects its performance compared to that of LMOF-202. Our research provides constructive information for the future exploration of LMOF-201 as a potential adsorbent. The H-bonding observed in LMOF-201 is important in the future studies of the gaseous mixtures as certain adsorbates do not exhibit H-bonding and effective functionalization of other MOFs to control the flexibility of MOFs.

Conflicts of interest

There are no conflicts to declare.

Acknowledgements

This work was supported by the JST-CREST, Grant Number JPMJCR17I3, Japan. DS was financially supported by the Iron and Steel Institute of Japan (ISIJ Research Promotion Grant).

Notes and references

1 H.-C. “Joe” Zhou and S. Kitagawa, *Chem. Soc. Rev.*, 2014, **43**, 5415–5418.
2 O. K. Farha, I. Eryazici, N. C. Jeong, B. G. Hauser, C. E. Wilmer, A. A. Sarjeant, R. Q. Snurr, S. T. Nguyen, A. Ö. Yazaydin and J. T. Hupp, *J. Am. Chem. Soc.*, 2012, **134**, 15016–15021.
3 M. Agrawal and D. S. Sholl, *ACS Appl. Mater. Interfaces*, 2019, **11**, 31060–31068.
4 M. Witman, S. Ling, S. Jawahery, P. G. Boyd, M. Haranczyk, B. Slater and B. Smit, *J. Am. Chem. Soc.*, 2017, **139**, 5547–5557.
5 N. Aljammal, C. Jabbour, S. Chaemchuen, T. Juzsakova and F. Verpoort, *Catalysts*, 2019, **9**, 512.
6 J. Heinen and D. Dubbeldam, *Wiley Interdisciplinary Reviews: Computational Molecular Science*, 2018, **8**, e1363.
7 N. A. Ramsahye, G. Maurin, S. Bourrelly, P. L. Llewellyn, T. Loiseau, C. Serre and G. Férey, *Chem. Commun.*, 2007, No. 31, 3261–3263.
8 D. Dubbeldam, R. Krishna and R. Q. Snurr, *J. Phys. Chem. C*, 2009, **113**, 19317–19327.
9 M. Agrawal, S. Bhattacharyya, Y. Huang, K. C. Jayachandrababu, C. R. Murdock, J. A. Bentley, A. Rivas-Cardona, M. M. Mertens, K. S. Walton, D. S. Sholl and N. Sankar, *J. Phys. Chem. C*, 2018, **122**, 386–397.
10 F. Salles, A. Ghoufi, G. Maurin, R. G. Bell, C. Mellot-Draznieks and G. Férey, *Angew. Chemie - Int. Ed.*, 2008, **47**, 8487–8491.
11 E. García-Pérez, P. Serra-Crespo, S. Hamad, F. Kapteijn and J. Gascon, *Phys. Chem. Chem. Phys.*, 2014, **16**, 16060–16066.
12 F. Salles, S. Bourrelly, H. Jobic, T. Devic, V. Guillerm, P. Llewellyn, C. Serre, G. Ferey and G. Maurin, *J. Phys. Chem. C*, 2011, **115**, 10764–10776.
13 A. Ghoufi, A. Subercaze, Q. Ma, P. G. Yot, Y. Ke, I. Puente-Orench, T. Devic, V. Guillerm, C. Zhong, C. Serre, G. Férey and G. Maurin, *J. Phys. Chem. C*, 2012, **116**, 13289–13295.
14 Q. Ma, Q. Yang, A. Ghoufi, G. Férey, C. Zhong and G. Maurin, *Dalt. Trans.*, 2012, **41**, 3915–3919.
15 A. Ghoufi and G. Maurin, *J. Phys. Chem. C*, 2010, **114**, 6496–6502.
16 J. Yu, L. H. Xie, J. R. Li, Y. Ma, J. M. Seminario and P. B. Balbuena, *Chem. Rev.*, 2017, **117**, 9674–9754.
17 S. Hiraide, H. Tanaka, N. Ishikawa and M. T. Miyahara, *ACS Appl. Mater. Interfaces*, 2017, **9**, 41066–41077.
18 S. Hiraide, H. Tanaka and M. T. Miyahara, *Dalton Transactions*, 2016, **45**, 4193–4202.
19 Q. Yang, D. Liu, C. Zhong and J. R. Li, *Chem. Rev.*, 2013, **113**, 8261–8323.
20 M. D. Allendorf, C. A. Bauer, R. K. Bhakta and R. J. T. Houk, *Chem. Soc. Rev.*, 2009, **38**, 1330–1352.
21 N. D. Rudd, H. Wang, E. M. A. Fuentes-Fernandez, S. J. Teat, F. Chen, G. Hall, Y. J. Chabal and J. Li, *ACS Appl. Mater. Interfaces*, 2016, **8**, 30294–30303.
22 Z. Hu, B. J. Deibert and J. Li, *Chem. Soc. Rev.*, 2014, **43**, 5815–5840.
23 Z. Hu, K. Tan, W. P. Lustig, H. Wang, Y. Zhao, C. Zheng, D. Banerjee, T. J. Emge, Y. J. Chabal and J. Li, *Chem. Sci.*, 2014, **5**, 4873–4877.
24 Y. Ma, Y. Harada, A. Hori, Y. Hijikata, L. Li and R. Matsuda, *Dalt. Trans.*, 2017, **46**, 15200–15203.
25 L. Huang, K. L. Joshi, A. C. T. V. Duin, T. J. Bandosz and K. E. Gubbins, *Phys. Chem. Chem. Phys.*, 2012, **14**, 11327–11332.
26 L. Huang, T. Bandosz, K. L. Joshi, A. C. T. Van Duin and K. E. Gubbins, *J. Chem. Phys.*, 2013, **138**, 034102.
27 S. S. Han, S. H. Choi and A. C. T. Van Duin, *Chem. Commun.*, 2010, **46**, 5713–5715.
28 Y. Yang, Y. K. Shin, S. Li, T. D. Bennett, A. C. T. Van Duin and J. C. Mauro, *J. Phys. Chem. B*, 2018, **122**, 9616–9624.
29 D. Dubbeldam, S. Calero, D. E. Ellis and R. Q. Snurr, *Mol. Simul.*, 2016, **42**, 81–101.
30 S. L. Mayo, B. D. Olafson and W. A. Goddard, *J. Phys. Chem.*, 1990, **94**, 8897–8909.
31 A. K. Rappé, C. J. Casewit, K. S. Colwell, W. A. Goddard and W. M. Skiff, *J. Am. Chem. Soc.*, 1992, **114**, 10024–10035.
32 L. Zhang and J. I. Siepmann, *Theor. Chem. Acc.*, 2006, **115**, 391–397.
33 S. Plimpton, *J. Comput. Phys.*, 1997, **117**, 1–42.

A table of contents entry

Molecular simulation study on the flexibility in the interpenetrated metal–organic framework LMOF-201 using reactive force field

Ankit Agrawal, [a] Mayank Agrawal, [b] Donguk Suh [a], Yunsheng Ma, [c,d] Ryotaro Matsuda, [c] Akira Endo, [e] Wei-Lun Hsu, [a] and Hirofumi Daiguji*[a]

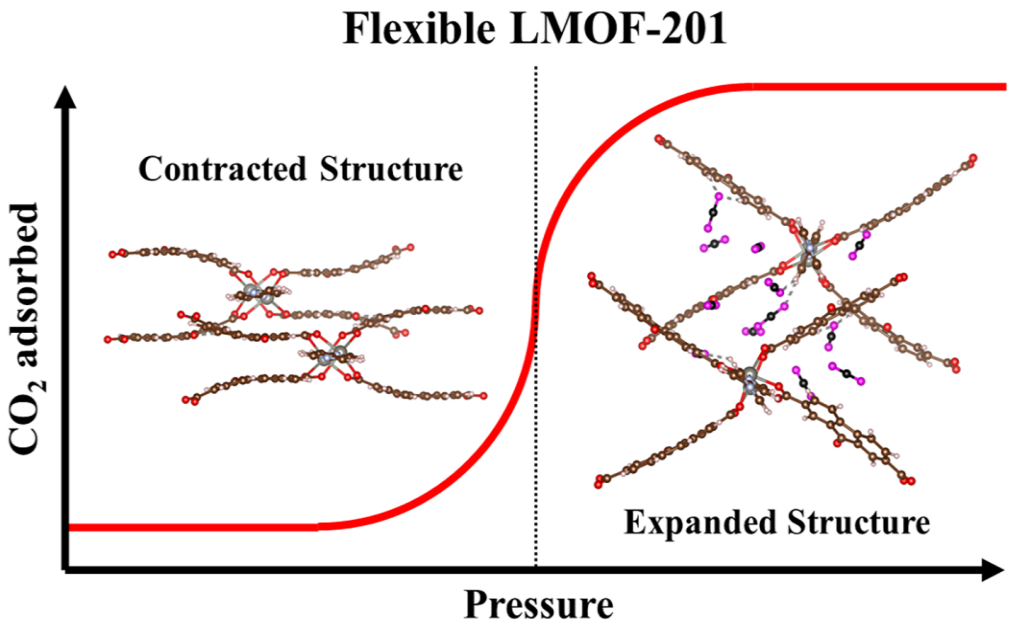

The guest-induced structural changes in LMOF-201 were demonstrated by using reactive force field combined with Grand Canonical Monte Carlo and molecular dynamics simulations.